Paper No. 2080. (quote when citing this article)
Eleventh World Conference on Earthquake Engineering
ISBN: 0 08 042822 3

NONLINEAR DYNAMIC SOIL PROPERTIES BACK-CALCULATED FROM STRONG SEISMIC MOTIONS DURING HYOGOKEN-NANBU EARTHQUAKE

T. KOKUSHO*, K. SATO*and M. MATSUMOTO**

* Central Research Institute of Electric Power Industry, Abiko, Japan
**Kansai Electric Power Company, Osaka, Japan

ABSTRACT

During the 1995 Hyogoken-Nanbu earthquake, vertical array records were obtained at four sites with much different epicentral distances in and around the earthquake fault zone. These acceleration records demonstrated conspicuous nonlinearity effect in seismic response due to different input accelerations. These vertical array records are analyzed in this research by means of the inversion technique to back-calculate dynamic soil properties exhibited during the strong earthquake motion. The shear modulus and damping ratio back-calculated for soils in four sites are found to show clear strain-dependency. The modulus and damping thus obtained for soil layers of different soil types in four sites have been plotted against effective strain to have clearly different strain-dependent curves for different types of soil. The back-calculated curves are also in accordance to those measured in laboratory tests for corresponding soil types.

KEY WORDS

Site amplification; nonlinear response;back-calculation; shear modulus; damping; liquefaction; lab test

INTRODUCTION

Local site amplification is one of the most important factors in the definition of the seismic ground motion for seismic zonation study. The site amplification is correlated to properties of soil layers such as soil densities, wave velocities and material dampings. At the same time it is expected to be highly dependent on the nonlinearity of soil properties in soft soil sites in particular.

Nonlinear seismic response of soft ground due to nonlinear soil properties had been evaluated numerically either by equivalent linear analyses (e.g. Schnabel 1972) or by step-by step nonlinear analyses (e.g. Constantopoulos et al. 1973) for the past two decades. In model tests, Kokusho et al. (1979) performed a shake table tests of a model ground in a laminar shear box of about one meter in depth consisting of fine sand and demonstrated a very clear reduction in dynamic amplification due to increasing input acceleration level. The same authors also compared the test results with the equivalent linear analysis based on the soil properties of the model ground to find a fair agreement between them. More recently several centrifuge shake table tests have been conducted for sand layers in laminar shear boxes to find clear amplification reduction with increasing acceleration again. Thus, the nonlinearity of site amplification due to strong input motions is obviously shown in numerical analyses and model tests. However, due to absence of vertical array records during strong earthquakes, not many seem to have believed the nonlinear seismic response to actually occur in the local site amplification. During the earthquake in Kobe, valuable earthquake records have been obtained to demonstrate and evaluate nonlinear amplification of soil ground, which will be studied from the viewpoint of dynamic soil properties in this research.

SITE CONDITION AND SEISMIC AMPLIFICATION

Vertical arrays which could record the mainshockof the 1995 Hyogoken-Nanbu earthquake (M=7.2) were located in four sites in the coastal zone around the Osaka-Bay area as shown in Fig.1. The same figure also indicates the fault zone including the epicenters of the mainshock as well as aftershocks. The four sites were very properly distributed by chance in terms of distances from the fault zone which can be estimated from the aftershock epicenters plotted in Fig.1. PI (the Port Island) array belonging to the Kobe Municipal Office was located just next to the fault zone, while other three arrays SGK, TKS and KNK belonging to the Kansai Electric Power Company are approximately 15km, 35km and 65km far from the fault zone respectively. The soil profiles and the depth of three dimensional down-hole seismographs are shown for the four sites in Fig.2 together with P and S-wave velocities measured by the down-hole logging method and SPT N-values along the depth. The deepest seismographs at the base layers of the four sites were located GL-83m in PI, GL-97m in SGK, and GL-100m in TKS and KNK respectively, and the geological condition there were Pleistocene dense gravelly soils except for KNK consisting of a hard rock.

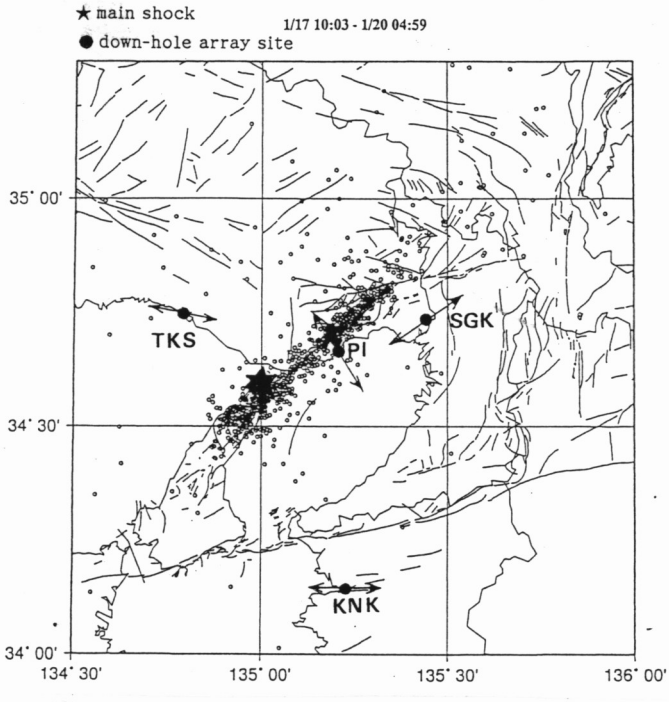

Fig.1 Location of vertical array sites around Osaka Bay and epicenters of mainshock and aftershocks

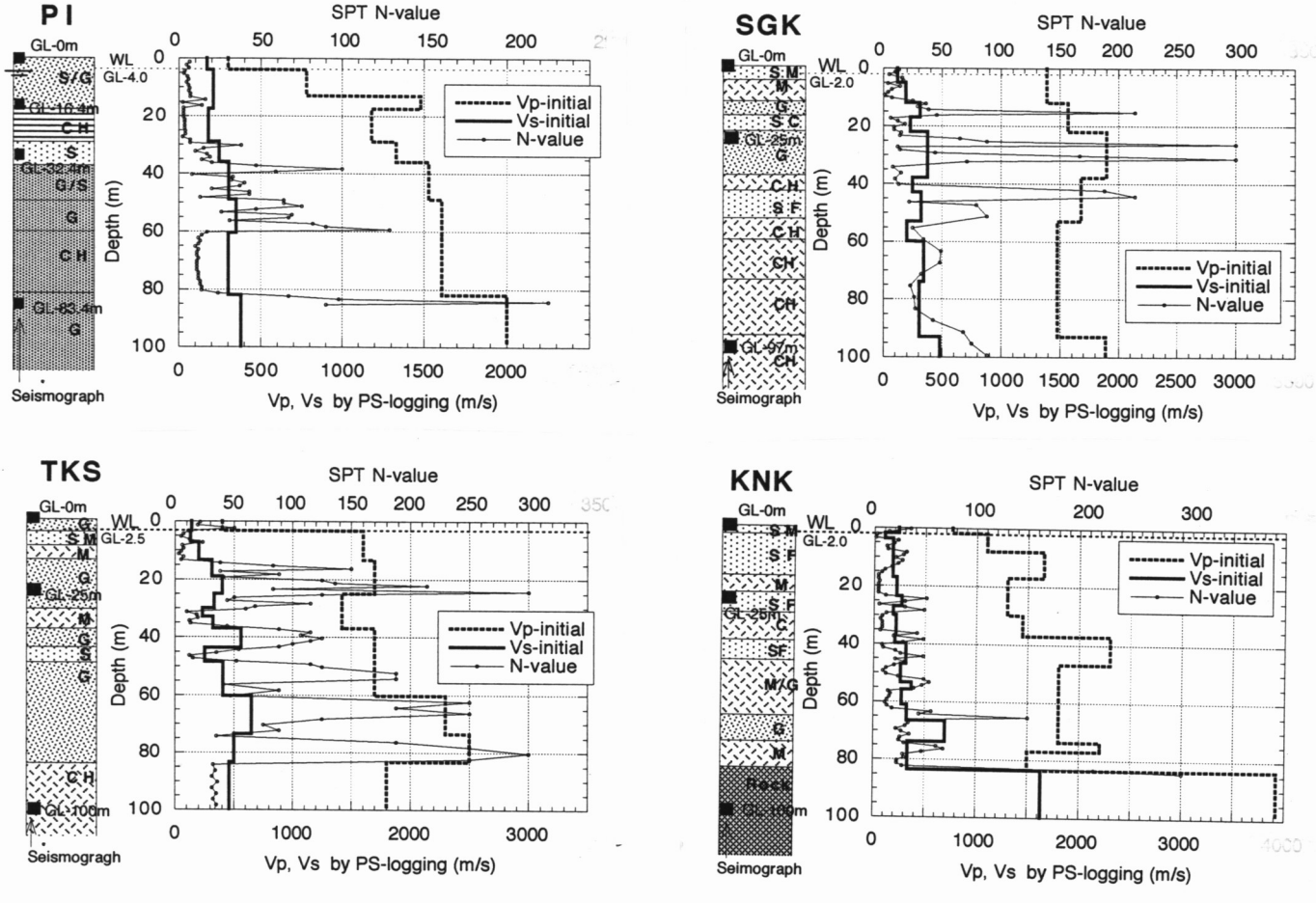

Fig.2 Soil profiles , wave logging test results and SPT N-values at four down-hole array sites

Upper soil conditions at the four sites are rather similar as shown in Fig.2, consisting of sandy fill at the surface in most sites underlain by Holocene clay and/or sand and further underlain by Pleistocene soils. The S-wave velocity, Vs, at the base layer of Pleistocene gravelly soil in PI, SGK and TKS is 380-480 m/s while Vs at the base rock in KNK is as high as 1630 m/s.

In Fig.3, down-hole distribution of maximum acceleration in two horizontal (NS,EW) and one vertical directions (UD) at the four sites are shown. The maximum accelerations at the deepest level are different in a wide range (from 26gal in KNK to 679gal in PI) in the four sites, leading to obvious difference in amplification in upper layers. In horizontal direction the amplification between the surface and the deepest level was 4 to 5 in KNK, while in TKS it was about 2 for the acceleration of 100gal at the bottom. It was between 1 to 2 for the acceleration of about 300gal and about one half in PI for the accelerations of 300 to 680gal. In PI, the surface sandy fill layer experienced very extensive liquefaction during the main-shock which obviously led to the damping in the maximum acceleration in the upper sandy fill layer.

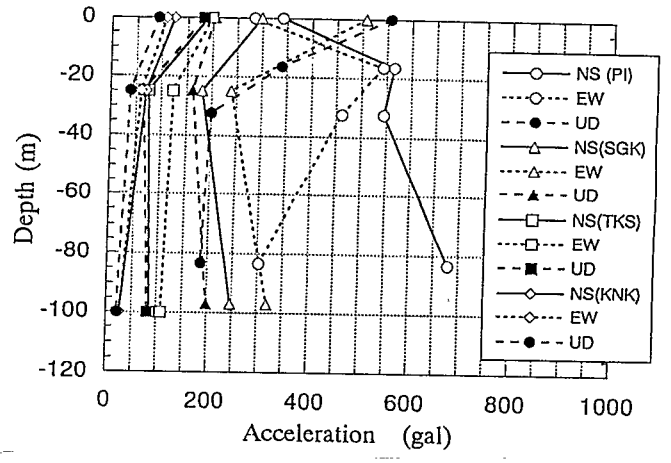

Fig.3 Distribution of maximum acceleration along depth at vertical array sites

INVERSION ANALYSES

The mainshock records obtained in the vertical arrays in the four sites were first examined to know directional drift of the buried seismographs in the horizontal plane (Sato et al. 1995). This examination revealed the following directional drifts or errors; a) 15 degrees clockwise rotation at GL-83.4m in PI, b) reverse in the NS-component at GL0m and 34 degrees anti-clockwise rotation at GL-97m in SGK, c) 30 degrees anti-clockwise rotation at GL-25m in TKS and d) reverse in the EW-component and 60 degrees clockwise rotation at GL0m in KNK. All data were accordingly corrected for later analyses except for the PI record in which 15 degrees of rotation was judged to have negligible effects on subsequent analyses.

A computer code used for the inversion analyses was originally developed by Ohta[1975], in which multi-reflection of vertically propagating SH-wave in a horizontally layering system is assumed. In the analysis tranfer functions (Fourier spectrum ratio) between measured seimic motions at different levels were developed. Next, a soil layer model was made with given thickness and density of each layer based on bore-hole data. Then starting from initial guess, the S-wave velocity, Vs, and the damping ratio, h were back-calculated so that the transfer functions of recorded motions be best reproduced by the soil layer model. Only the absolute value of the transfer function was used for the back-calculation. The initial guess for the S-wave velocity was made by reducing the measured Vs indicated in Fig.2 by some amount according to estimated strain-dependent velocity reduction. For the damping ratio laboratory cyclic loading test data were referred for the initial guess.

PI records

At first remarkable nonlinear seismic response in PI where the surface fill layer extensively liquefied were analyzed. Thick lines in Fig.4 show measured time histories in twenty seconds for the mainshock in two horizontal and one vertical directions at four levels. In Fig.5, transfer functions between two measured motions at different four levels in Fig.3 are shown in NS and EW directions with thin lines. The transfer functions best reproduced by the inversion analysis are illustrated with thick lines in Fig.5. The degree of the reproduction of the transfer functions was judged so that peaks in lower frequency are better reproduced by the back-calculation than higher frequency peaks especially in transfer functions for shallower layers. .

In Fig.6, S-wave velocities, Vs, back-calculated for the major portion of the time history in the mainshock (T=20 seconds) are plotted together with initial values corresponding to the wave logging test against the depth for NS and EW directions. In NS direction, optimized Vs is approximately 20% and 40% smaller than the initial value for the Pleistocene and Holocene layer respectively. For the fill layer, 80% and 50% reduction of Vs can be identified for saturated and unsaturated layer respectively presumably because of the

extensive liquefaction in the fill.

In the same diagram, Vs distribution optimized only for a partial time history (T=5.12s, from 4.10s to 9.22s in Fig.4) in which SH-wave is dominant in the measured time history is also shown. No meaningful difference can be seen between the results for the total time and the partial time, implying that reliable soil properties can be back-calculated from the total time history although different types of waves such as P and S-wave and surface waves are all together involved in it [Sato et al. 1995]. Based on this finding, only the major portions of time histories (T=20s for PI and SGK, T=40 for TKS and KNK) were chosen in all records for the back-calculation of properties hereafter.

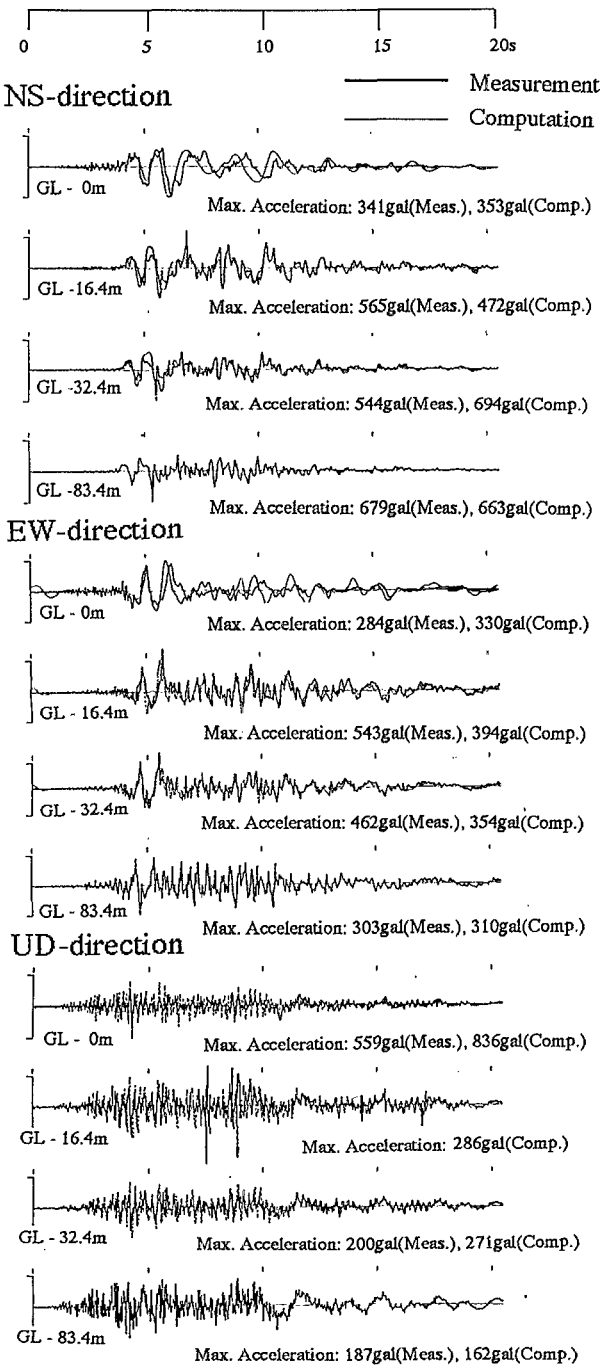

Fig.4 Measured and computed acceleration time histories at PI

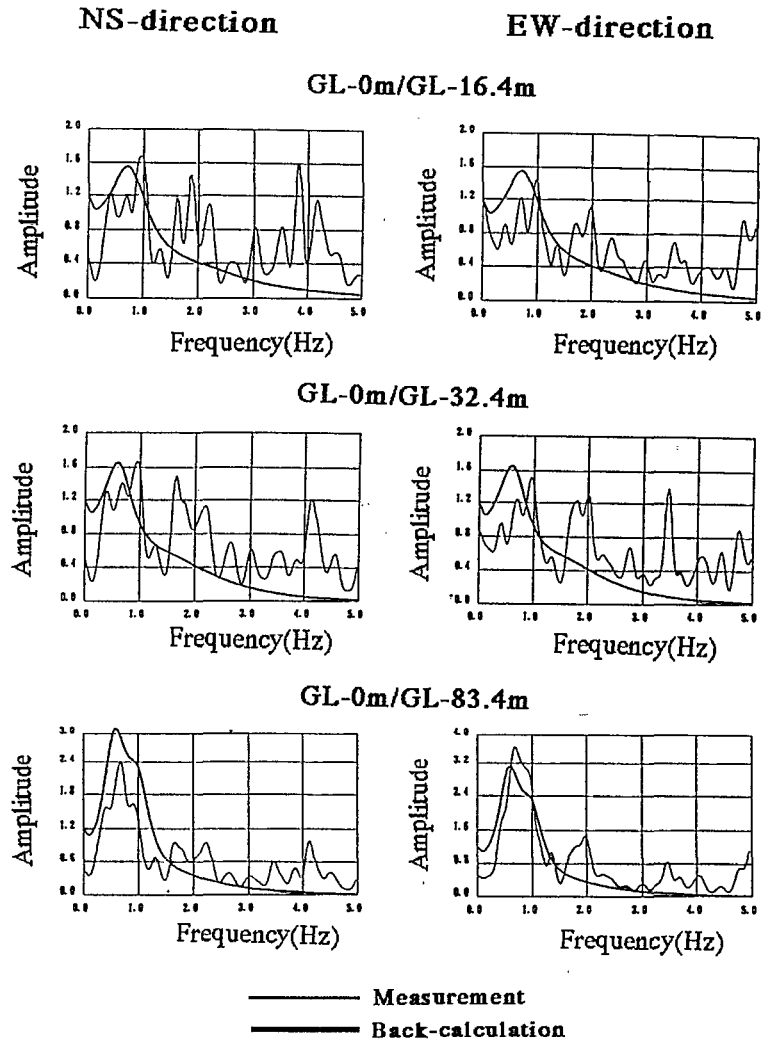

Fig.5 Measured and back-calculated transfer functions for horizontal motions at PI

Another interesting results can be obtained from the analysis for an aftershock with maximum surface acceleration of about 0.01G which occurred only about two minutes after the main-shock. As shown in the graph, Vs for Pleistocene and Holocene layers can be interpreted to have returned to the initial value because of small magnitude of the induced strain during the after-shock while those in the fill layer take almost the same reduced value as the main-shock, indicating the liquefaction in the fill was still sustained. With regard to the main-shock in the EW direction in Fig.6, the reduction rate of Vs is a little smaller than that in the NS direction because of the smaller input acceleration, while for the aftershock the result is exactly the same as that in the NS direction including the reduced Vs in the liquefied fill layer.

For the vertical acceleration, a similar inversion analysis was carried out based on a postulate that vertical seismic motion can be explained by the multi-reflection theory of vertically propagating P-wave. Fig.7 shows the result optimized for a time interval (T=5.12s, from 0s to 5.12ss in Fig.4) in which the P-wave motion looks most dominant. Despite some small difference of Vp from that of the wave logging test, it may be concluded that P-wave velocity changes little with the intensity of acceleration except for the unsaturated fill layer where Vp is reduced by 50%. This result seems to confirm the theoretical basis of P-wave propagation through a saturated porous media in which no change in effective stress takes place.

Fig.8 indicates the damping ratio, h, for horizontal motions in NS and EW directions, respectively. For the mainshock, h is optimized as 6% for the Pleistocene soils and the Holocene sand layer and as high as 33 to 50% for the upper layer, indicating that equivalent damping ratio for the liquefied layer is evaluated very high. The optimized h for the aftershock is evidently larger; 5% for the Pleistocene soils and 10 to 12% for Holocene and fill layers compared with the initial value estimated from previous laboratory test data for small strain range also shown on the diagram. The same trend has also been pointed out in a previous investigation [kokusho 1992]. Very little has so far been investigated for the damping ratio exerted in P-wave propagation. Also shown in Fig.8 is the damping ratio back-calculated for the vertical motion, which is optimized as 5 to 6% in all saturated layers up to the fill layer, while it is evaluated as 10% in unsaturated fill.

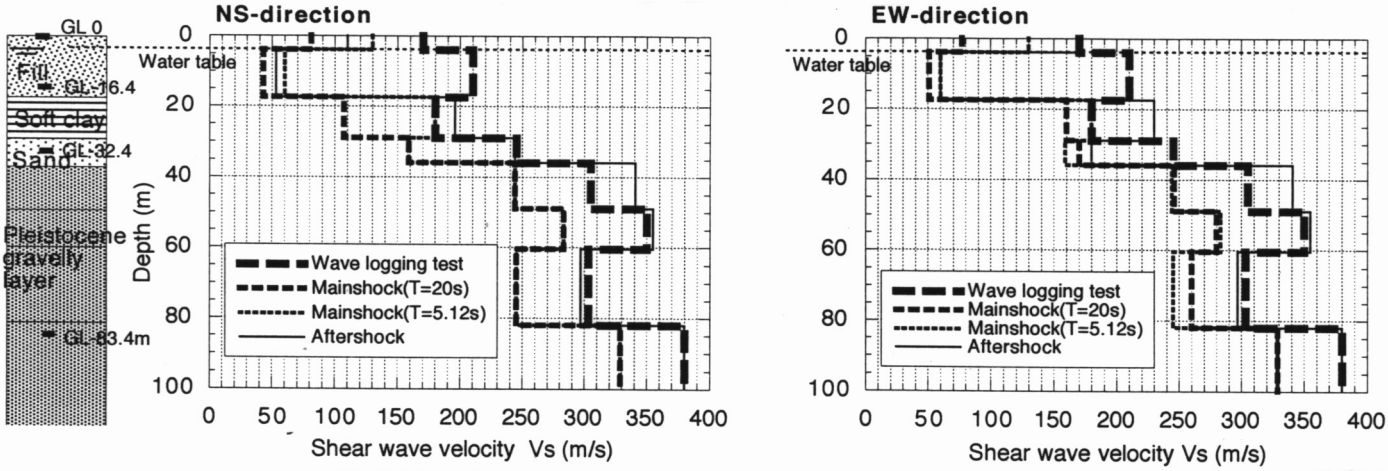

Fig.6 Back-calculated S-wave velocity for NS and EW-motions compared with wave logging test at PI

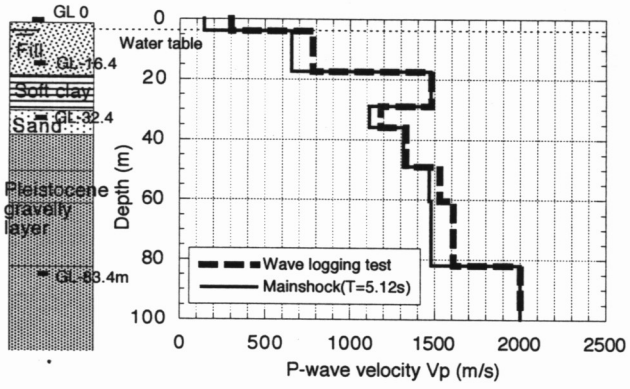

Fig.7 Back-calculated P-wave velocity for vertical motion compared with wave logging test at PI

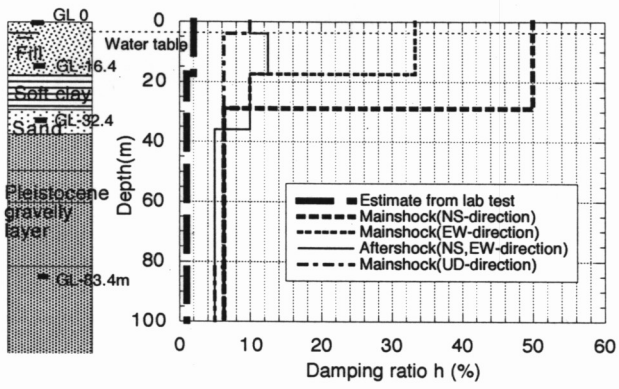

Fig.8 Back-calculated damping ratio for horizontal and vertical motions compared with lab test value at PI

A normal multi-reflection analysis of the mainshock has been carried out based on the optimized properties to compare the results with the measurement. In Fig.4, time histories of upper three levels computed from the lowest level are indicated with thin lines. The agreement between analysis and measurement is quite satisfactory in the middle two levels and also for the surface level despite some visible phase lag of the measured wave compared to the analysis probably due to the liquefaction of the fill layer. In Fig.9 computed max. shear strains, γ_{max}, are shown against the depth for two horizontal directions, which indicate the shear strain evaluated by the equivalent linear analysis exceeds 1 to 2% in the liquefied fill layer while in other layers it stays within much smaller value.

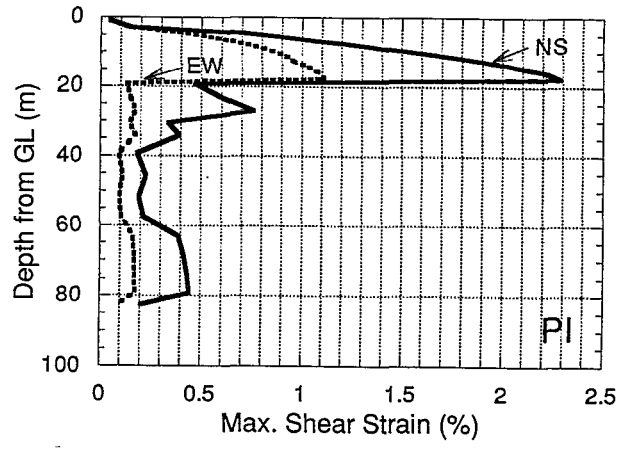

Fig.9 Computed max. shear strain along depth at PI

SGK records

In this site no trace of liquefaction such as sand eruptions, ground fissures, soil subsidence, etc. was found after the earthquake. In Fig.10, time histories of T=20s in two horizontal directions obtained in the vertical array in SGK are shown with thick lines. In Fig.11, transfer functions between two measured time histories at different levels are shown with thick lines. The thin lines in this figure indicate back-calculated transfer function which, in this case too, is regulated to have better matching for lower frequency peaks than for higher ones.

The S-wave velocity, Vs, and the damping ratio, h, back-calculated in two directions are taken against the depth in Fig.12. In upper Holocene and Pleistocene layers of silts or sands, reduction rate in Vs compared with Vs corresponding to those in PS-logging is evaluated as 30 to 50% while in lower Pleistocene layers it is less than 20%. The damping ratio amounts to 2 to 6% in the Pleistocene soils in contrast to mostly more than 10% in Holocene soils.

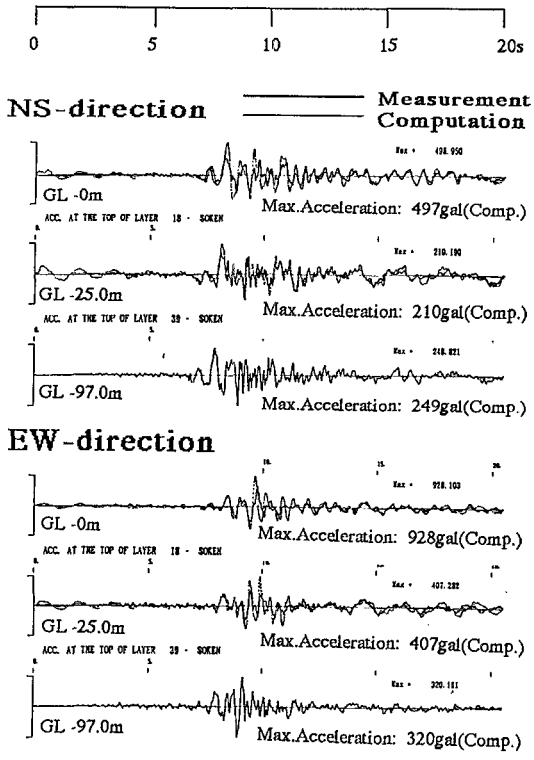

Fig.10 Measured and computed acceleration time histories at SGK

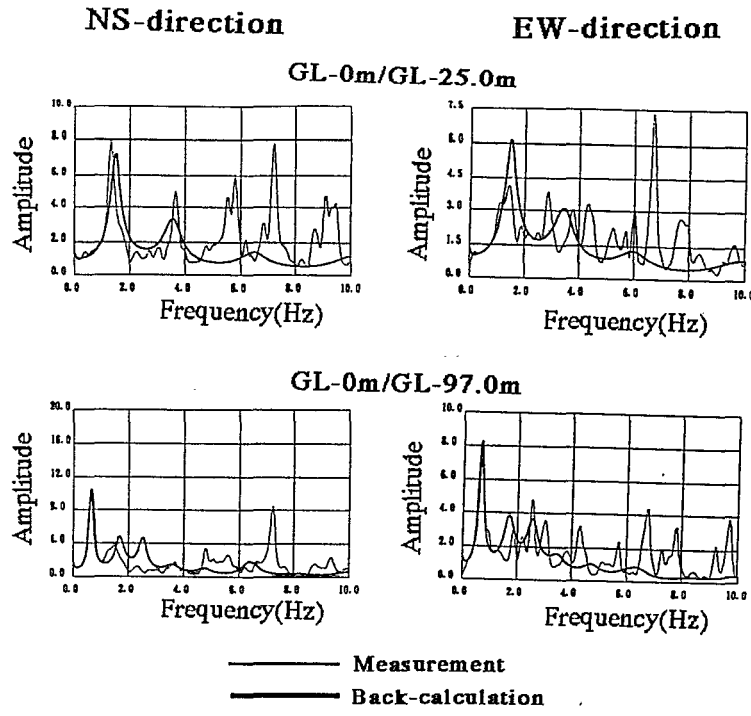

Fig.11 Measured and back-calculated transfer functions for horizontal motions at SGK

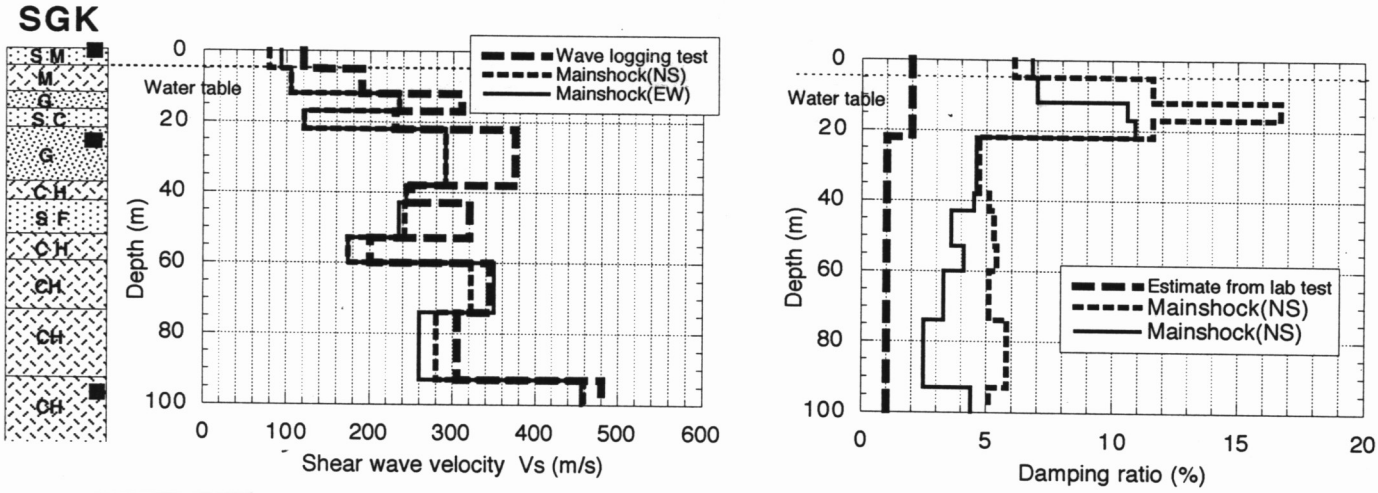

Fig.12 Back-calculated S-wave velocity and damping ratio at SGK

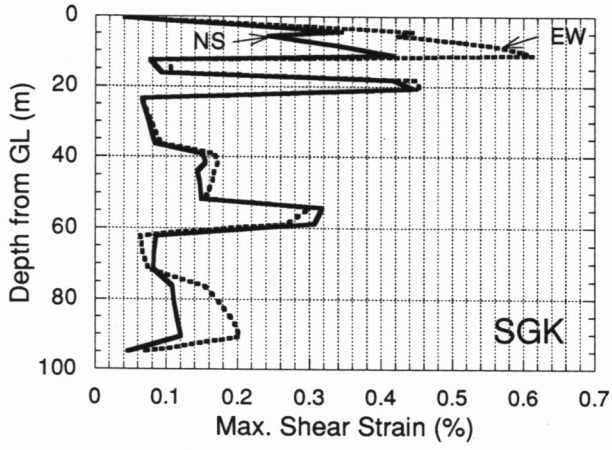

Fig.13 Computed max. shear strain along depth at SGK

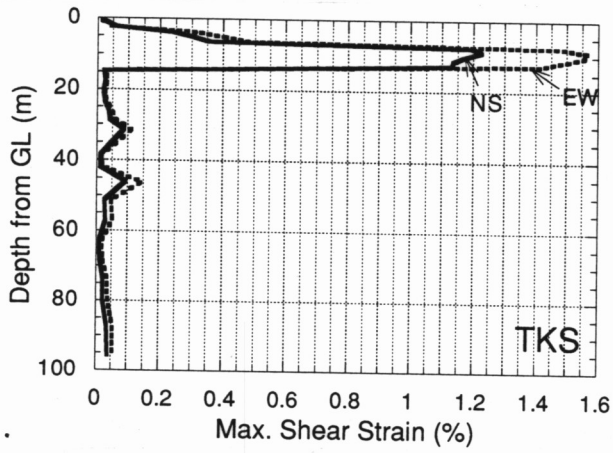

Fig.17 Computed max. shear strain along depth at TKS

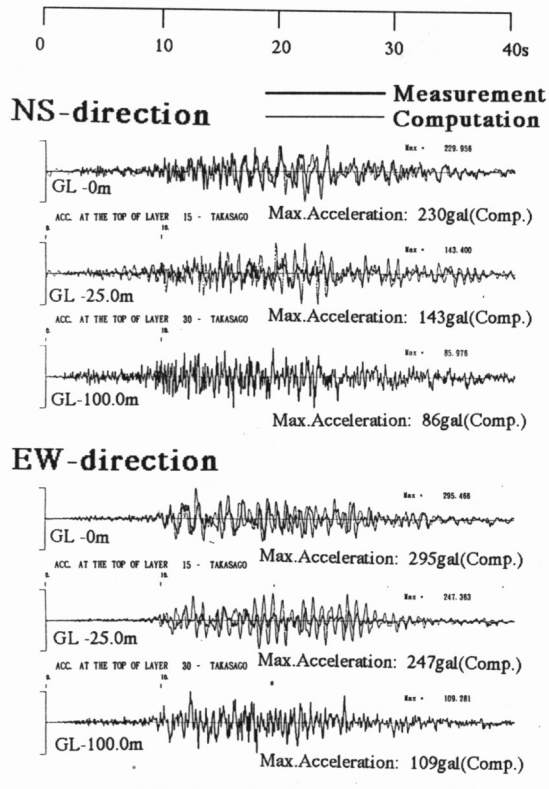

Fig.14 Measured and computed acceleration time histories at TKS

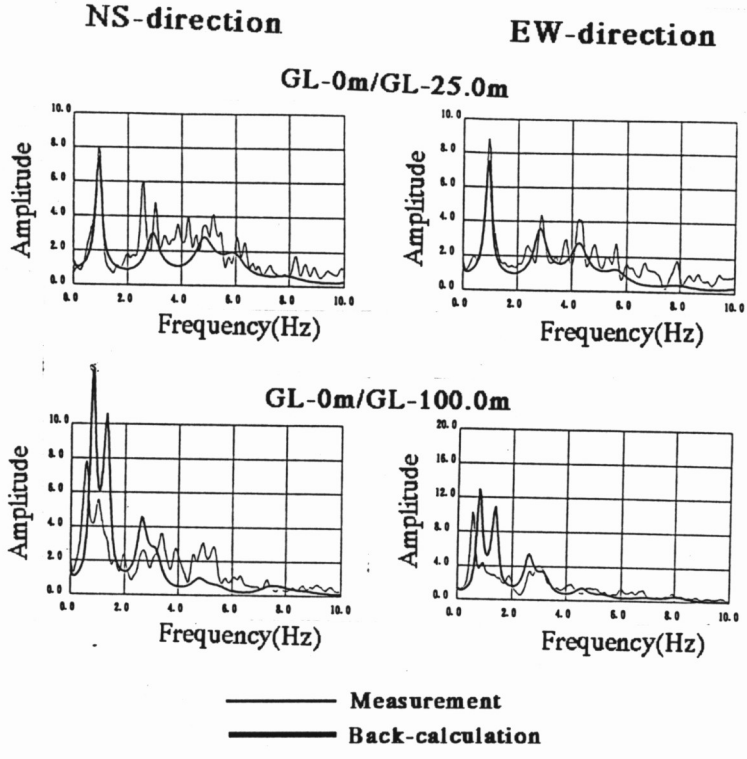

Fig.15 Measured and back-calculated transfer functions for horizontal motions at TKS

The computed time histories based on the back-calculated properties are compared with the measurements in Fig.10, in which the agreement of wave forms seems good though the computed maximum acceleration somewhat overestimates the measurement. Fig.13 indicates computed max. strain distribution along the depth, indicating that the max. strain, γ_{max}, stays within 0.6%, smaller than PI, probably because the liquefaction did not take place in this site.

TKS records

In this site soil eruptions and fissures were witnessed after the earthquake indicating the occurrence of liquefaction near the surface. Fig.14 shows the measured time histories of T=40s at three levels in two directions with the thick lines. The longer time period of T=40s was taken in TKS and KNK because the major portion of the seismic motion was longer there due to longer epicentral distance. In Fig.16, transfer functions between two measured motions at two different levels are illustrated with thin lines. The thick lines in the same figure represent back-calculated transfer functions, indicating better agreement in the upper portion of the ground.

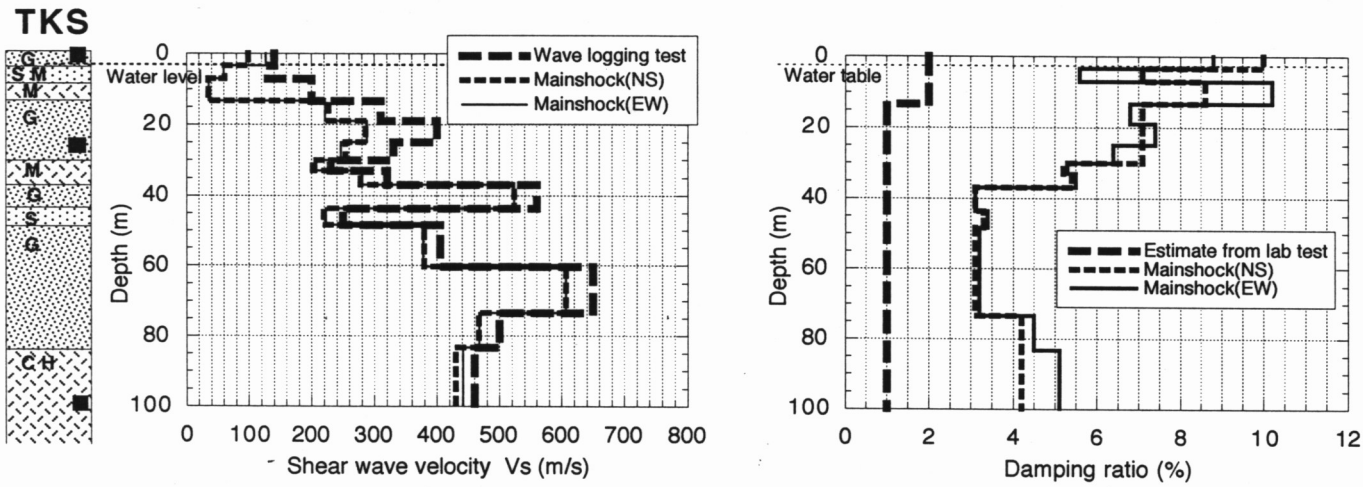

Fig.16 Back-calculated S-wave velocity and damping ratio at TKS

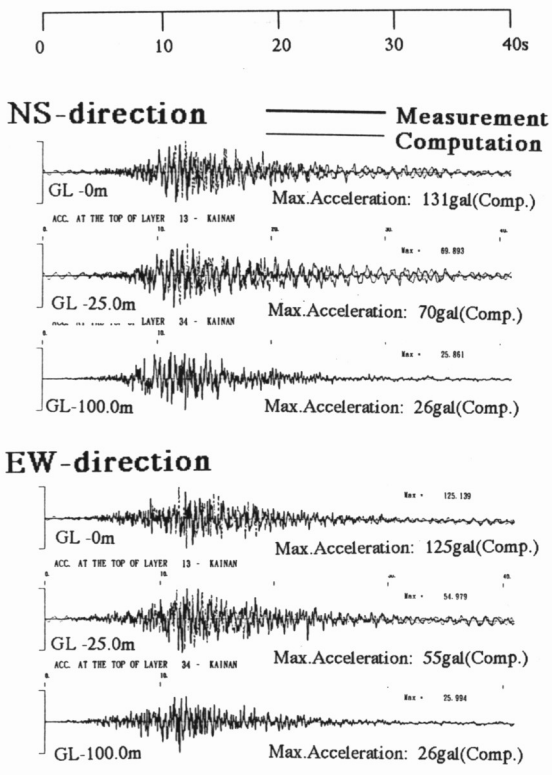

Fig.18 Measured and computed acceleration time histories at KNK

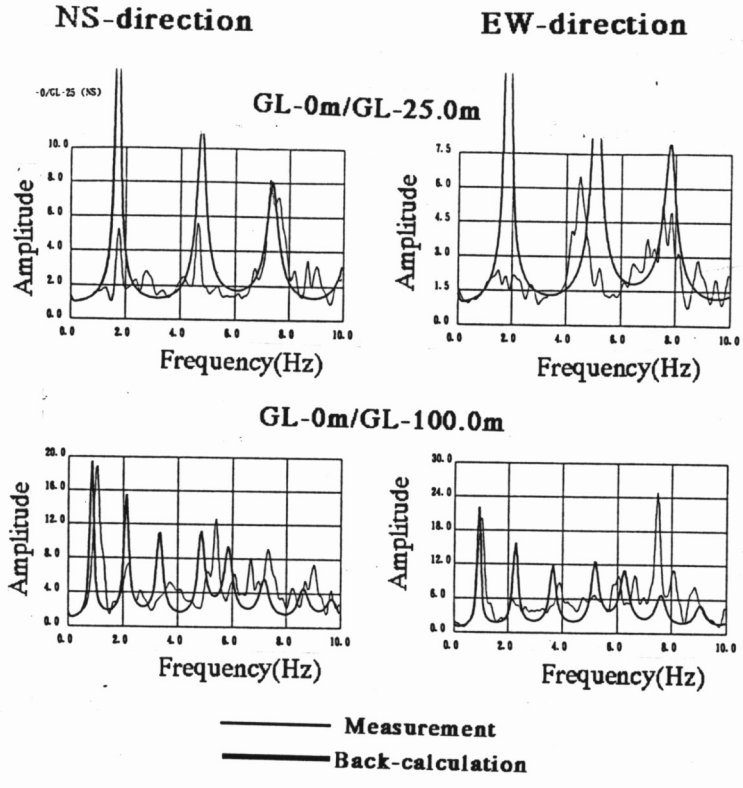

Fig.19 Measured and back-calculated transfer functions for horizontal motions at KNK

S-wave velocities and damping ratios back-calculated for NS and EW directions are plotted against the depth in Fig.17. Vs is drastically reduced from initial Vs corresponding to wave logging test more than 80% and 50% in silt and silty sand between GL-3m and GL-13m, indicating the occurrence of liquefaction in these layers, whereas in the layers below the reduction rate is less than 25% and mostly less than 10%. The damping ratio is evaluated as 3 to 5% in the lower layers and even in the liquefied upper layers it is back-calculated as 6 to 10% in contrast to 33 to 50% in the liquefied soil in PI.

The computed time-histories based on these optimized values are compared with measured ones in Fig.14. In Fig.17, computed max. strain, γ_{max}, in NS and EW directions is illustrated along the depth, which clearly indicates remarkably large strain of 1.2 to 1.6% induced in the seemingly liquefied layer.

KNK records

With epicentral distance of 65km, the max. acceleration at the base rock in this site was about 0.025G, resulting in almost linear response in the soil layers. Fig.18 shows measured time histories of T=40s at three levels with thick lines. In Fig.19 show transfer functions between measured motions at two different levels with thin lines. The thick lines in the same figure indicate back-calculated results, which do not appear to agree very well in some peaks.

S-wave velocities and damping ratios back-calculated for NS and EW directions are plotted against the depth in Fig.20. Vs is reduced from the initial values by maximum 20% in the upper layers while in the lower layers the reduction rate is less than 5%. h takes 1% in the layers deeper than 40m and about 2% in the upper layers except in the very shallow part where h is evaluated as about 4%.

The computed time-histories based on these optimized values are compared with measured ones in Fig.18. In Fig.21, computed max. strain, γ_{max}, in NS and EW directions is illustrated along the depth, which indicates only very limited induced strain of less than 0.06% in KNK site.

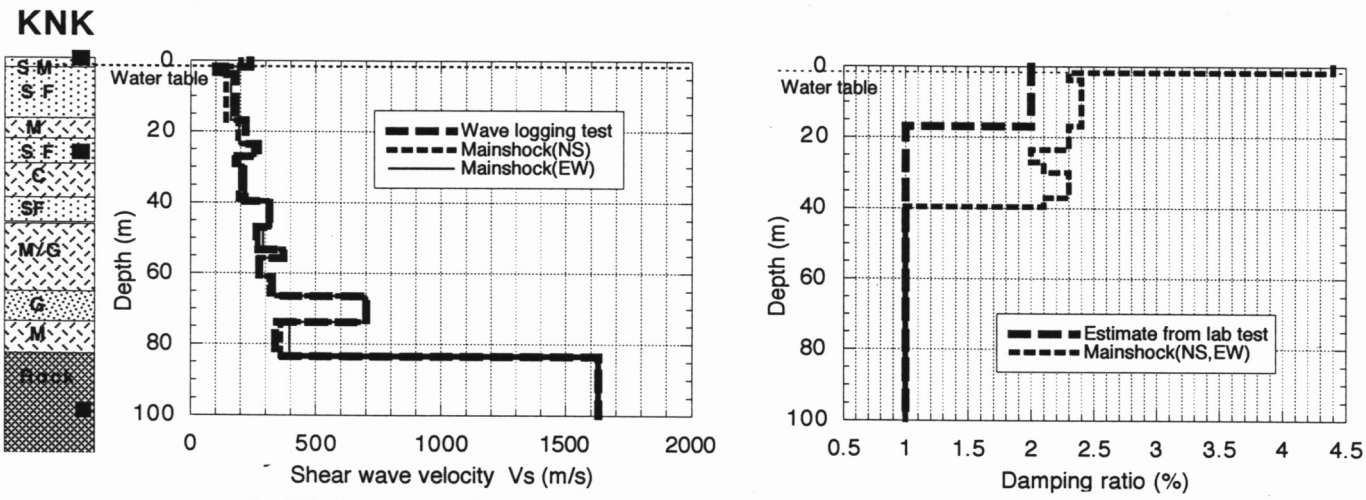

Fig.20 Back-calculated S-wave velocity and damping ratio at KNK

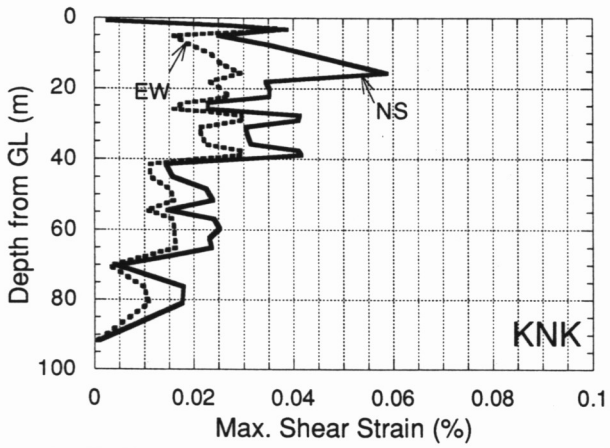

Fig.21 Computed max. shear strain along depth at KNK

BACK-CALCULATED STRAIN-DEPENDENT SOIL PROPERTIES

Based on the back-calculation for dynamic soil properties best reproducing site responses in the four vertical array sites, it becomes possible to synthesize strain-dependent curves of modulus degradation and damping ratio. The shear modulus ratio, G/G_0, where G and G_0 are shear modulus for a certain strain level and the initial modulus for infinitely small strain, respectively, can be readily calculated as the square of the Vs-ratio between the back-calculation and the wave logging test based on the results indicated in Figs.6, 12, 16 and 20. Effective shear strain, γ_{eff}, corresponding to a modulus degradation may be assumed 2/3 of maximum strain, γ_{max}, in a similar manner as often employed in design practice and can be calculated from the max. strain distributions as shown in Figs.9, 13, 17 and 20.

The shear modulus ratios thus calculated in NS and EW directions for all individual soil layers in the soil profiles in the four sites are plotted against the logarithm of the corresponding effective strain in Fig.22. The plots with the arrow marks correspond to soil layers where liquefaction fully or partially took place during the earthquake. By excluding these plots and also several other plots exceeding $G/G_0=1.0$, the modulus degradation can obviously be represented by the chain-dotted curves in the gragh. Those points which exceed $G/G_0=1.0$ all belong to KNK site, implying that some review, in the optimized properties or in the site investigation results might be needed.

The damping ratios back-calculated in NS and EW directions for all individual soil layers in the soil profiles in the four sites are plotted against the logarithm of the corresponding effective strain in Fig.23. Although some plots are of very high damping ratios representing the liquefied layer in PI, there exists evident trend of increasing damping with the increase of effective strain.

In order to know difference in strain-dependent variations of modulus and damping ratio for different soil types, these data are further classified into four soil types; clay, silt, sand and gravel, based on original descriptions in boring logging data sheets. Fig.26 shows the same plots of modulus degradation as in Fig.22 but with different symbols representing the four types of soil. It may be judged from this figure that modulus degradation curves can obviously be separated into different groups according to different soil types; the degradation curve for clays is positioned in the most right-hand side and that for gravels in the most left-hand side while silts and sands are located between the two. In the same manner, damping ratios are shown only for the damping value less than 20% and classified into the four soil types in Fig.27. This figure also indicates clear trend of strain-dependent damping variation which is unique to each type of soil: clay is the most rightward, gravel the most leftward and others in between.

Numerous laboratory tests have been conducted to date to measure the strain-dependent changes of modulus and damping on many types of soil. Based on those data modulus degradation curves for clay and sand may be represented for example by Fig.24 (Kokusho et al. 1982 and Kokusho et al. 1980). It is obviously seen that the curve for sand is positioned more left hand-side than that for clay on the gragh and for sand the curves tend to shift to the right with the increase of confining stress. For clay the curve, which is insensitive to the difference in confining stress, tends to shift from an original position for non-plastic soil

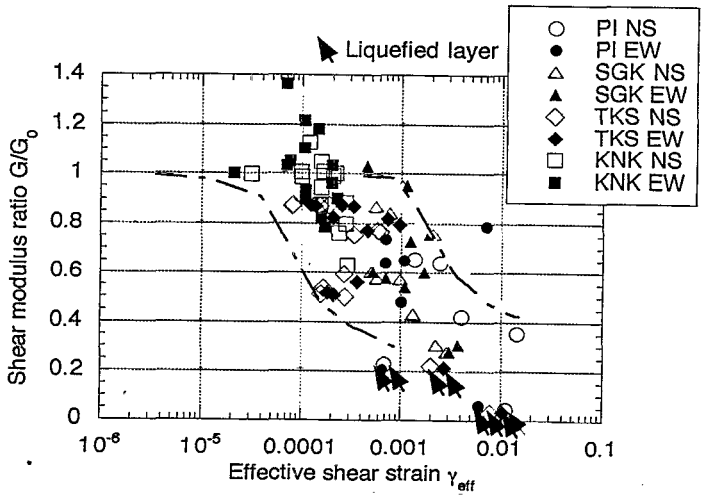

Fig.22 Shear modulus ratio versus effective strain charts obtained from back-calculation at four sites

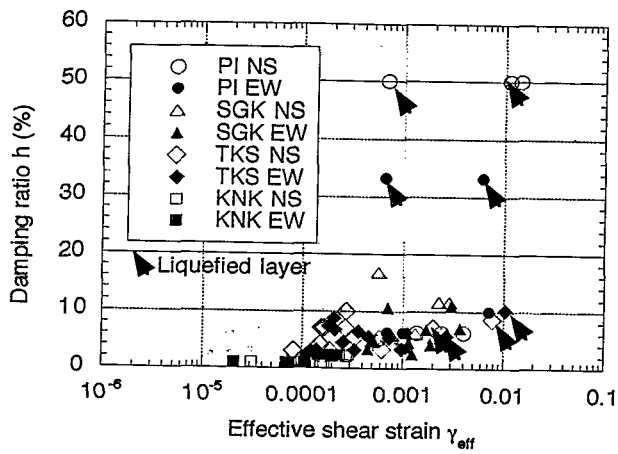

Fig.23 Damping ratio versus effective strain charts obtained from back-calculation at four sites

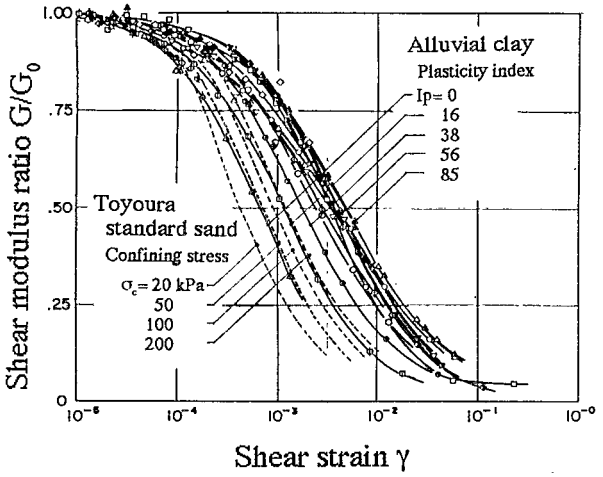

Fig.24 Laboratory test results on shear modulus degradation for clay and sand

(sand) to the right with the increase of the plasticity index, PI. For gravels, as shown in Fig.25(a), the curves are positioned more left than sand and clay, and also shift with varying confining pressure (Kokusho et al. 1994). For damping ratio, laboratory test data for gravel are shown compared with other soil types in Fig.25(b), indicating that the same trend as the modulus degradation curve seems to exist for the damping curves for different soil types and confining stress.

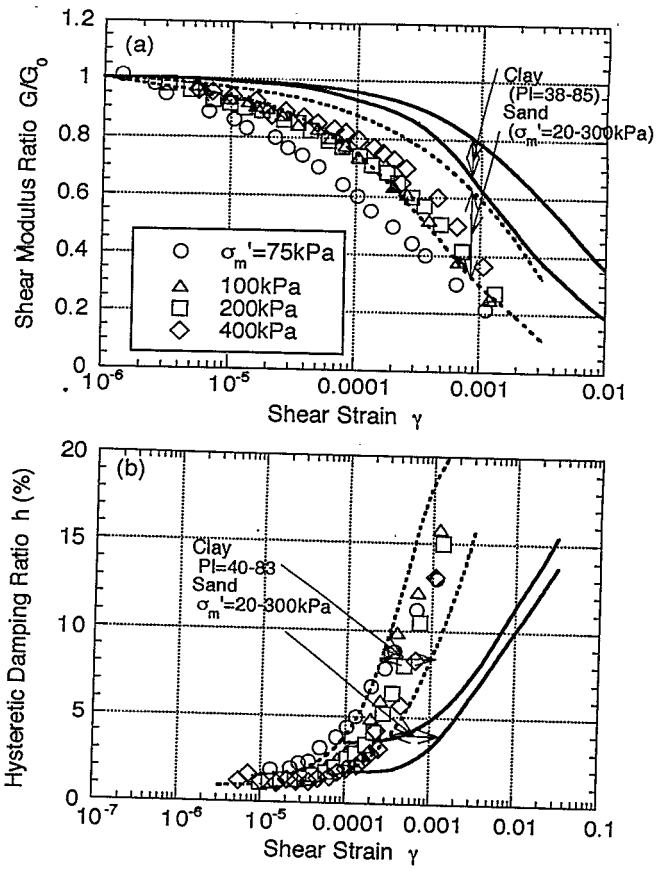

Fig.25 Laboratory test results on strain-dependency of modulus and damping for gravel

In Figs.26 and 27, modulus degradation curves and strain-dependent damping variation curves by laboratory tests discussed above are drawn for gavel, sand and clay to compare with the back-calculation. In comparing the laboratory properties with the back-calculated in-situ properties, the followings should be borne in mind; The plasticity indices of clays around the Osaka bay area take a wide range between 100 and 20, with their majority falling in between 80 and 40 while the lab test data are for PI=40 to 83. The interval of in-situ confining stress for sands may be approximated as 20 to 300kPa, which coincides with that of the lab test data. Because of the great depth of gravel layers in PI, TKS and KNK site, the interval of in-situ confining stress for gravels is likely to exceed the higher stress limit of 400kPa for the lab test data. Though there exist certain amounts of scatters in back-calculated properties, relatively good agreement can be recognized between field back-calculations and laboratory tests, demonstrating that laboratory dynamic soil properties can be applicable to the evaluation of nonlinear site response during strong earthquakes.

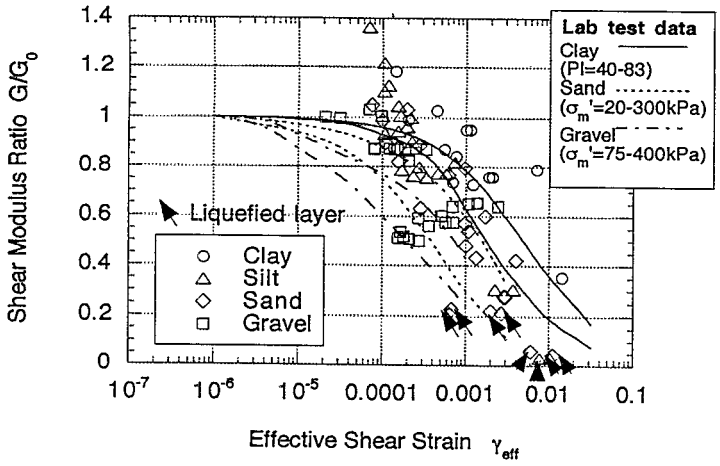

Fig.26 Shear modulus ratio versus effective strain charts classified for four soil types

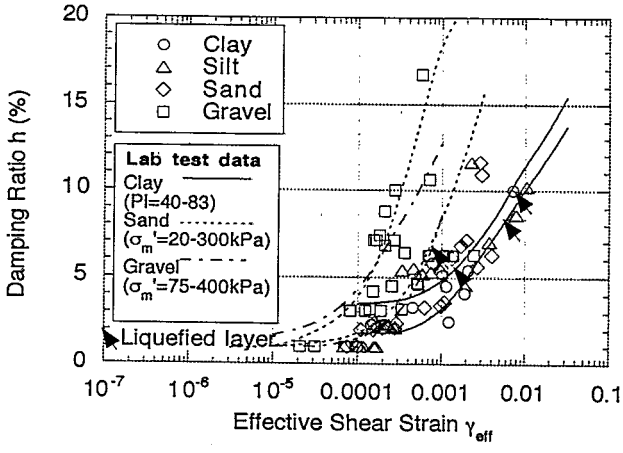

Fig.27 Damping ratio versus effective strain charts classified for four soil types at four sites

exhibited site amplification of soil ground with different levels of nonlinearity due to different levels of input acceleration. By making use of these data-base the inversion analyses have been carried out to back-calculate optimum soil properties which can best reproduce the measured soil response. Based on these calculations, the following conclusions have been reached.

1. In liquefied layers in PI and TKS, back-calculated S-wave velocity was reduced by 80 to 50% from the initial value while, in other non-liquefied layers in four sites, the reduction in Vs was maximum 40% or less.

2. S-wave velocity optimized for a small aftershock which occurred two minutes after the mainshock had already returned to the initial value for non-liquefied layer, whereas in the liquefied layer the reduction in Vs during the mainshock was still sustained, implying the continuation of liquefaction.

3. Inversion analysis for vertical motions in PI clearly indicates that P-wave velocity is virtually unaffected by input acceleration level, confirming the theoretical basis for P-wave propagation in a saturated porous media.

4. Strain-dependent variations in the shear modulus and the damping ratio were derived from back-calculated soil properties in four sites, from which different strain-dependency curves can be separated for clay, silt, sand and gravel.

5. The strain-dependency curves back-calculated for different soil types were found to well agree with those by laboratory tests, demonstrating that nonlinear dynamic soil properties measured in the laboratory can be applicable to numerical analyses for nonlinear site response during strong earthquakes.

ACKNOWLEDGMENTS

The earthquake records used in this research have been provided by the Kansai Earthquake Observation Association chaired by Professor Kenzo Toki of Kyoto University. The authors gratefully appreciate their activities and kindness.

REFERENCES

Constantopoulos,I.V., Roesset,J.M. and Christian, J.T. (1973) " A comparison of linear and exact nonlinear analyses of soil amplification, Proc. 5th International Conference on SMFE, Rome,1806-1815

Kokusho,T. and Iwatate,K. (1979) "Scaled model tests and numerical analyses on nonlinear dynamic response of soft grounds" Journal of Japan Society for Civil Engineers (in Japanese), No.285,57-67

Kokusho,T. (1980) "Cyclic triaxial test of dynamic soil properties for wide strain range" Soils and Foundations, Vol.20, No.2, 45-60

Kokusho,T., Yoshida,Y. and Esashi,Y. (1982) "Dynamic soil properties of soft clay for wide strain range", Soils and Foundations, Vol.22, No.4, 1-18

Kokusho,T., Tohma,J., Yajima,Y., Tanaka,Y., Kanatani,M. and Yasuda,N.(1992) "Seismic response of soil layer and its dynamic properties" Proc. 10WCEE, Madrid,6671-6680

Kokusho,T. and Tanaka,Y.(1994) "Dynamic properties of gravel layers investigated by in-situ freezing sampling" ASCE Convention (Atlanta), Geotechnical Special Publication No44 -Ground Failures under Seismic Conditions, pp121-140

Ohta,H.(1975) "Application of optimization method to earthquake engineering (Part I) -Estimation of underground structure of SMAC observation site in Hachinohe Harbor-" Journal of Japan Society of Architectural Engineering (in Japanese)

Sato,K., Kokusho,T., Matsumoto,M. and Yamada,E.(1996) " Nonlinear seismic response and soil property during 1995 Hyogoken Nanbu earthquake" Soils and Foundations (to be published) Special Issue for the Hyogoken Nanbu earthquake, January

Schnabel, P.B., Lysmer,J. and Seed, H.B.(1972) "SHAKE, A computer program for earthquake response analysis of horizontally layered sites" Report EERC 72-12, University of California Berkeley